Journal Name

ARTICLE TYPE

Cite this: DOI: 10.1039/xxxxxxxxxx

Spin-glass–like aging in colloidal and granular glasses

Beatriz Seoane*[a,b] and Francesco Zamponi[a]

Received Date
Accepted Date

DOI: 10.1039/xxxxxxxxxx

www.rsc.org/journalname

arXiv:1803.05031v2 [cond-mat.soft] 23 Apr 2018

Motivated by the mean field prediction of a Gardner phase transition between a "normal glass" and a "marginally stable glass", we investigate the off-equilibrium dynamics of three-dimensional polydisperse hard spheres, used as a model for colloidal or granular glasses. Deep inside the glass phase, we find that a sharp crossover pressure $P_{\rm G}$ separates two distinct dynamical regimes. For pressure $P < P_{\rm G}$, the glass behaves as a normal solid, displaying fast dynamics that quickly equilibrates within the glass free energy basin. For $P > P_{\rm G}$, instead, the dynamics becomes strongly anomalous, displaying very large equilibration time scales, aging, and a constantly increasing dynamical susceptibility. The crossover at $P_{\rm G}$ is strongly reminiscent of the one observed in three-dimensional spin-glasses in an external field, suggesting that the two systems are in the same universality class, consistently with theoretical expectations.

1 Introduction

The Gardner transition is an exotic spin-glass phase transition that was discovered independently in 1985 by Gardner[1] and by Gross, Kanter, and Sompolinsky[2]. It happens in a broad range of mean field spin-glass models, that belong to the discontinuous random first order transition (RFOT) universality class[3–7]. The physics of these models is the following. At high temperature T, there is a single paramagnetic phase. Upon lowering the temperature, a discontinuous *dynamical glass transition* is met at $T = T_{\rm d}$, at which the dynamics become arrested, while the equilibrium properties display no singularity. At any temperature $T < T_{\rm d}$, a large number of infinitely long-lived metastable glassy states are present. These states fully trap the dynamics and ergodicity is broken, but if prepared inside any of them, the system can fully equilibrate in a short time. One can then prepare a system in equilibrium in the arrested phase, at an initial temperature $T_{\rm g} < T_{\rm d}$, and change the temperature to a value $T < T_{\rm g}$. The system remains confined in the original glass state, whose evolution can thus be followed in a restricted, metastable equilibrium[8–12]. During this process, each individual state might undergo a continuous spin-glass phase transition at a temperature $T_{\rm G}(T_{\rm g}) < T_{\rm g}$, called the Gardner transition[10,11,13,14]. Below the Gardner transition, $T < T_{\rm G}(T_{\rm g})$, the glass state is described by a full replica symmetry broken (fullRSB) structure, discovered by Parisi[15], that also describes the low-temperature phase of usual mean field spin-glasses[16].

The RFOT universality class is known to provide a mean field theory for the structural glass transition of particle systems[17–24]. In particular, a d-dimensional hard sphere liquid in the limit of $d \to \infty$ realises precisely the RFOT scenario[17,25–29], with temperature T being replaced, as control parameter, by packing fraction φ or pressure P. Yet, despite the fact that *(i)* the analogy between the structural glass transition and RFOT spin-glass models, and *(ii)* the presence of a Gardner transition in the latter models, are both well known since the 80s, no attempt to look systematically for a Gardner transition in structural glasses has been made, until very recently.

The situation changed dramatically when it was realised that hard sphere glasses, close to the jamming transition[30–32] (i.e. the infinite pressure limit), are *marginally stable*[33–41]. Marginal stability is naturally described, at the mean field level, by the Parisi fullRSB construction[16], thus motivating the search for a Gardner transition in structural glasses. Such a transition was indeed found[27,29] in the limit $d \to \infty$. It was then found[29,42,43] that the resulting fullRSB construction in $d \to \infty$ provides an accurate quantitative description of the criticality and marginality of jamming in any dimension $d \geq 2$, leading to the conjecture[44] that the lower critical dimension for jamming might be equal to $d = 2$.

The existence of a Gardner transition to a fullRSB phase in structural glasses might have deep implications for their properties. In fact, marginal stability strongly affects the low-frequency vibrational density of states[45–47], the elastic[48] and rheological[49–53] properties of the solid, and its low-temperature transport properties[54]. These theoretical results motivated the proposal that marginal stability could be a unifying principle behind many anomalies of amorphous solids[27,39,41,45], and the search for a Gardner transition in a broad range of systems, both in numerical simulations[51,55–58] and experiments[59,60]. Currently, it is

[a]Laboratoire de physique théorique, Département de physique de l'ENS, École normale supérieure, PSL Research University, Sorbonne Universités, CNRS, 75005 Paris, France; [b]Instituto de Biocomputación y Física de Sistemas Complejos (BIFI), 50009 Zaragoza, Spain.
*E-mail: beaseobar@gmail.com

believed that $3d$ Lennard-Jones–like systems, that are good models for metallic and molecular glasses, generically do not show a Gardner transition[57,58], while $3d$ hard sphere systems, that are good models for granular and colloidal glasses, display several anomalies at high pressures[51,55,56], that suggest the existence of a sharp Gardner crossover, if not a true transition. However, a careful investigation of the nature of both the crossover and the new phase has not yet been performed.

In this work, we clarify the nature of the Gardner crossover in $3d$ hard sphere glasses. We report a careful study of the off-equilibrium dynamics after an instantaneous compression ("crunch") from the equilibrium, dynamically arrested, supercooled liquid phase, to a state at higher pressure P, deep in the glass phase. For mild compressions, the dynamics relaxes to the metastable glass equilibrium on short times. For compressions to a higher pressure, a long time scale emerges. The dynamics is unable to ergodically sample the glass basin, it displays aging, and a growing correlation length.

We also present results for the $3d$ Edwards-Anderson spin-glass model with a magnetic field, which display the same qualitative behavior. We conclude that $3d$ spin glasses in a field and $3d$ colloidal glasses fall into the same universality class, as it happens in $d \to \infty$ and as it is generically expected from the theory, because in both systems there is no spontaneous symmetry breaking apart from the replica one[48,61–63]. In both systems, the dynamics becomes extremely slow around a crossover, due to a cooperative phenomenon associated to a growing correlation length, but the length grows so slowly (roughly logarithmically) with time that deciding whether a true divergence (i.e. a phase transition) or just a sharp dynamical crossover are observed is extremely tricky[64]. Note that the analogy between the dynamics of glasses and the $d = 3$ Edwards-Anderson spin-glass in a field had also been previously proposed in simulations (see Ref. 65), although in a different region of the phase diagram. Also, note that a RFOT theory of nucleation effects in hard spheres has been recently developed[66], which gives predictions about how marginal stability is modified in three dimensions.

Our results are interesting for the physics of colloidal and granular glasses, because they show that important dynamical anomalies are to be expected deep in the glass phase, consistently with the experimental results of Ref. 59. Moreover, we introduce a set of simple dynamical observables that can be measured in experiments to reveal the growing length and time scales associated to the Gardner crossover.

2 Simulation details, preparation protocol, and main observables

We simulate a system of N three-dimensional ($3d$) polydisperse hard spheres, precisely identical to the one investigated in Ref. 56, to which we refer for details. Most of the results are reported for $N = 1000$ but we also explored other sizes to quantify the finite size effects. All the quantities below are given in units of the mean particle diameter (length scale), the temperature (energy scale), and the particle mass (time scale)[56].

A set of initial configurations at three distinct packing fractions $\varphi_\ell = 0.565$, $\varphi_{g_1} = 0.619$ and $\varphi_{g_2} = 0.630$ (Fig. 1) have been prepared using an event-driven Molecular Dynamics (MD) code*, in which in addition to MD steps, from time to time particles are swapped, allowing for fast equilibration up to extremely high values of densities[67]. At density $\varphi_\ell = 0.565$, the relaxation time of the standard MD without swap is short compared with the accessible times, so the system is liquid. At densities φ_{g_1} and φ_{g_2}, the standard MD dynamics is much larger than the accessible times of the simulation, so the system is in a dynamically arrested supercooled liquid phase[67]. Note that in the following we will carefully distinguish a "dynamically arrested supercooled liquid", which is an equilibrium liquid whose relaxation time is much larger than the experimentally accessible time scale, from a "glass" which is a state obtained by compressing off-equilibrium a dynamically arrested system. For each initial density, $N_s = 20$ (40 for the highest pressures) independent equilibrium configurations have been prepared (both concerning the radii and the positions of the particles). We refer to these initial configurations as our "samples".

These initials configurations are used as input to a standard constant-pressure Monte Carlo (MC) code. The target pressure P of the MC code is set to a larger value than the initial equilibrium pressure, i.e. the system is instantaneously compressed ("crunched")[68,69] from the initial equilibrium pressure to the target pressure P. With the objective of fixing the time-scale and keeping the acceptance rate of the proposed volume dilation/contraction moves around 0.3, we fix $\delta V \propto 1/(PN)$ (note that the probability that two distinct particles overlap grows with the system size). In addition, we propose single particle moves randomly distributed within a sphere of radius $e^{-10R}\delta r$, where $R \in [0,1)$ is a uniformly distributed random variable, and $\delta r \propto L/P$ (to take into account that the cage size decreases linearly with the pressure), being L the linear size of the system. The random exponential term is introduced to encourage relaxation at high pressures, which requires both long and very short displacements. Note that with this choice of parameters, the bigger the system, the slower the compression of the system is after the quench, but once the volume has converged to its final value, there is almost no effect of N in the dynamics. We will come back to this point in Section 3.5.

Following Ref. 56, each equilibrium configuration is compressed independently (i.e. using a different seed for the random number generator of the MC code) several times, leading to a set of $N_c = 41$ (81 for the highest pressures) "clones" dynamically evolving at constant target pressure P. We denote by t_w the time elapsed since the initial crunch, and we measure the subsequent evolution of several observables as a function of time. Besides the instantaneous density $\varphi(t_w)$, following previous work[55–58], we focus our attention on the mean square displacement (MSD) of particles in each clone between time t_w and $t + t_w$, defined as

$$\Delta(t+t_w, t_w) = \frac{1}{N}\sum_{i=1}^{N} \overline{\left\langle |\vec{r}_i(t+t_w) - \vec{r}_i(t_w)|^2 \right\rangle}\,, \qquad (1)$$

* The swap-MD code has been written by Yuliang Jin who kindly provided us the initial equilibrated configurations, from Ref. 51.

This journal is © The Royal Society of Chemistry [year]

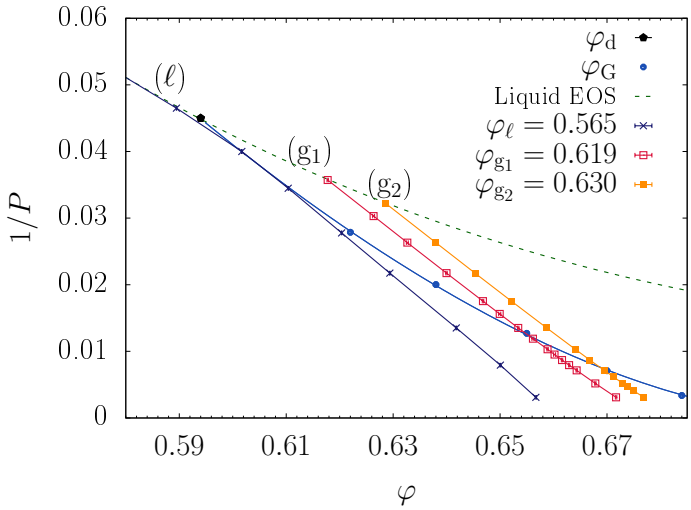

Fig. 1 Phase diagram. Phase diagram in the inverse pressure $1/P$ vs packing fraction φ plane. The dashed line is the supercooled liquid equilibrium equation of state, from Ref. 56, on which the three initial state points are selected at $\varphi_\ell = 0.565$, $\varphi_{g_1} = 0.619$ and $\varphi_{g_2} = 0.630$. The black pentagon marks the location of the dynamical glass transition φ_d, also from Ref. 56. The circles indicate the estimate of the Gardner crossover obtained in Ref. 56. The crosses, open squares, and full squares indicate the off-equilibrium equations of state obtained in this work, by compression from the three initial densities.

and the MSD between particles in two distinct clones (denoted A and B) of the same initial configuration at the same time t_w, $\{\vec{r}_i^A(t_w)\}$ and $\{\vec{r}_i^B(t_w)\}$, defined as

$$\Delta_{AB}(t_w) = \frac{1}{N}\sum_{i=1}^{N} \overline{\langle |\vec{r}_i^A(t_w) - \vec{r}_i^B(t_w)|^2 \rangle} \,. \quad (2)$$

In practice, to avoid spurious contributions from small particles diffusing in the holes of large ones, the sums over i have been restricted to the $N/2$ largest particles. Here, $\langle \bullet \rangle$ refers to the dynamical average, computed as the average over all the clones of the same sample, while $\overline{\bullet}$ refers to the average over all the samples with the same initial density. To increase the statistics, the dynamical average of Δ_{AB} is computed using all the $N_c(N_c-1)/2$ possible pairs of A and B clones, but the error bars are computed by taking into account the correlations between pairs using the jack-knife method[70].

In addition, we introduce the displacement of individual particles $u_i(t,t_w) = |\vec{r}_i(t+t_w) - \vec{r}_i(t_w)|^2$, and following Ref. 57 we introduce a susceptibility

$$\chi(t,t_w) = \overline{\left[\frac{\sum_{ij}[\langle u_i(t,t_w)u_j(t,t_w)\rangle - \langle u_i(t,t_w)\rangle\langle u_j(t,t_w)\rangle]}{\sum_i[\langle u_i(t,t_w)^2\rangle - \langle u_i(t,t_w)\rangle^2]}\right]} \,. \quad (3)$$

Similarly, defining $u_i^{AB}(t_w) = |\vec{r}_i^A(t_w) - \vec{r}_i^B(t_w)|^2$ as the relative displacement of two clones, we can introduce

$$\chi_{AB}(t_w) = \overline{\left[\frac{\sum_{ij}[\langle u_i^{AB}(t_w)u_j^{AB}(t_w)\rangle - \langle u_i^{AB}(t_w)\rangle\langle u_j^{AB}(t_w)\rangle]}{\sum_i[\langle u_i^{AB}(t_w)^2\rangle - \langle u_i^{AB}(t_w)\rangle^2]}\right]} \,. \quad (4)$$

Both susceptibilities, by their definition, are equal to 1 if u_i and u_j are uncorrelated for all $i \neq j$, while otherwise they give an estimate of the correlation length of particle displacements (raised to an unknown power). We found that, contrary to the standard wisdom in spin-glasses in equilibrium, the best way to decrease the statistical errors of the susceptibilities was to consider a large number of clones N_c, not a large number of samples N_s. This effect has been recently observed in non equilibrium spin-glasses as well[71].

Note that while the measurement of $\Delta_{AB}(t_w)$ and $\chi_{AB}(t_w)$ requires the artificial cloning procedure, which is very difficult (if not impossible) to implement in experiments, the measurement of $\Delta(t,t_w)$ and of $\chi(t,t_w)$ is straightforwardly achievable in experiments[59]. In the following we will present results for both kind of observables.

3 Results: hard spheres

3.1 Dynamics from the ergodic liquid phase

In Fig. 2a, we report the evolution of the packing fraction $\varphi(t_w)$ after a crunch from the liquid phase at initial density $\varphi_\ell = 0.565$. In this case, after a rapid growth on short times, the packing fraction continues to evolve slowly (almost logarithmically in t_w) and never reaches a stationary value. Note that for the largest pressure $P = 323$, the compactification dynamics starts to slow down considerably. This is due to our Monte Carlo procedure, in which despite our careful choice of moves, the proposed changes of volume are not accepted frequently enough at too high pressure. This limits the accessible range to $P \lesssim 400$. The values of φ for the largest t_w are reported in the phase diagram of Fig. 1. They form a line that originates from the equilibrium dynamical transition point $\varphi_d \approx 0.594$ (the point at which the equilibrium liquid relaxation time effectively diverges) and ends around $\varphi \approx 0.66$ at infinite pressure. In mean field, this line would correspond to the *threshold line*[13,14,29,72] where glassy metastable states first appear for a given pressure P. We would like to point out that the determination of this line depends on the time-window studied, although it is expected not to change too much as long as the original liquid state φ_ℓ is well below φ_d. As long as φ_ℓ approaches φ_d, the final point of the line, which corresponds to the jamming point, moves to higher values of φ, as discussed in Ref. 73. We have checked these results by simulating a second liquid line starting from liquid configurations at $\varphi_{\ell_2} = 0.59$ (data can be found in the Appendix). As expected, the new off-equilibrium equation of state also begins at φ_d but displays a slightly different slope, ending in a slightly higher value of φ. Yet, the dynamics along this second line are qualitatively very similar to those of $\varphi_\ell = 0.565$ so we will not discuss them any further. Nevertheless, for completeness we report a figure analogous to Fig. 2 for $\varphi_{\ell_2} = 0.59$ and $\varphi_{g_2} = 0.630$ in the Appendix.

In Fig. 2b, we report the evolution of the MSD $\Delta(t,t_w)$ for the same crunch from the liquid phase. As in the standard dynamics of glasses quenched from the liquid phase[22,23,72], upon increasing t_w, we observe the formation of a plateau at intermediate times t in the MSD, whose value becomes smaller with increasing t_w. For larger t_w, the plateau stabilises at its asymptotic value,

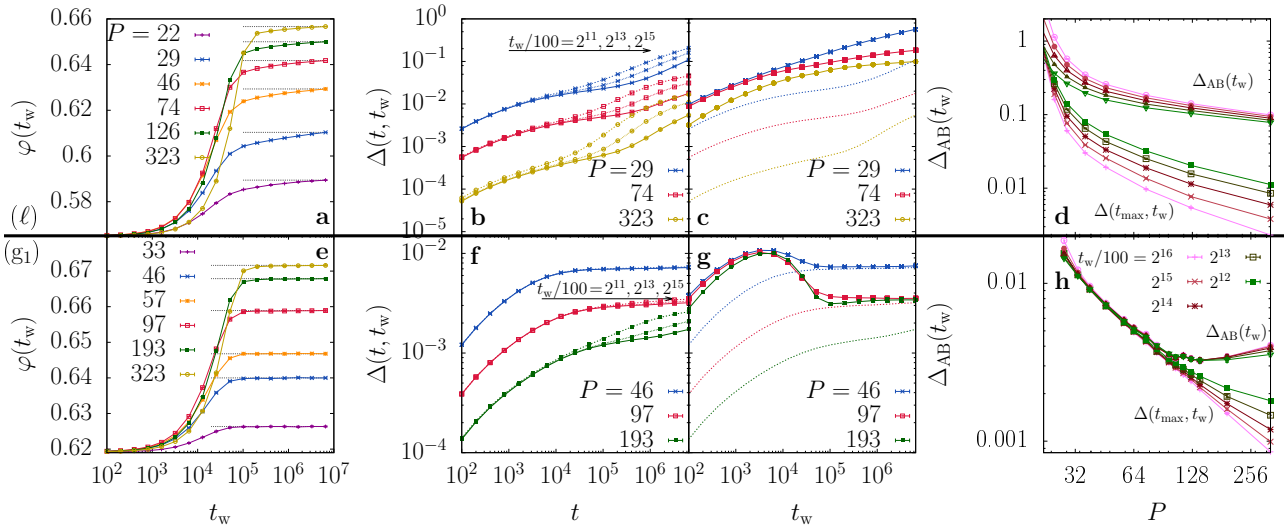

Fig. 2 Dynamics after a crunch. We show the evolution of different dynamical observables after a sudden crunch from the ergodic liquid ($\varphi_\ell = 0.565$) (top panels) and the dynamically arrested liquid ($\varphi_{g1} = 0.619$) (bottom panels). (a,e) **Densification dynamics:** evolution of the packing-fraction φ with t_w, the time elapsed since the quench, for different final pressures. While the liquid (a) displays extremely slow evolution, the glass (e) quickly converges to its final value. As a guide for the eye, we mark the last value of $\varphi(t_w)$ with a dashed horizontal line. (b,f) **Aging in the mean-squared-displacement (MSD):** we show $\Delta(t,t_w)$ for three final pressures P and three different t_w. Again, the liquid (b) displays traditional aging behavior for all the pressures, i.e. the development of a plateau of caging dynamics, followed by diffusion at longer times. The situation in the glass is different (f): at low pressures no aging or diffusion is observed in the simulated window of times, while strong non-diffusive aging is observed for pressures above a well defined crossover at $P \sim 97$. (c,d,g,h) **Ergodicity breaking:** Comparison between $\Delta(t,t_w)$ as function of t for the highest t_w ($t_w/100 = 2^{15}$) and the mean-squared distance between clones, $\Delta_{AB}(t_w)$ vs t_w. Because the liquid (c) does not display constrained dynamics at low pressures, the different clones are free to separate, giving, as a result, large values of Δ_{AB} even beyond the plateau of the MSD. On the contrary, in the glass (g), both Δ_{AB} and Δ converge to the same plateau value for $P \lesssim 97$, evidentiating the thermalization within the glass basin, while both values clearly differ at high pressures. In (d) and (h) we show (for different values of t_w) $\Delta(t_{max}, t_w)$, with t_{max} the higher t available for each t_w, and $\Delta_{AB}(t_w)$ as function of the pressure P. The splitting between Δ_{AB} and Δ at high pressures in the glass (h) suggests a breaking of ergodicity beyond the Gardner crossover.

but still at large t the MSD is observed to depend sensibly on t_w, which is the well-known phenomenon of *aging*[22,23,72]. Older glasses (larger t_w) display diffusive behavior at larger times t.

In Fig. 2c, we report the evolution of the MSD between clones, $\Delta_{AB}(t_w)$, for the crunch from the liquid. We observe that $\Delta_{AB}(t_w)$ quickly reaches large values, much larger than the individual $\Delta(t,t_w)$ of a single clone, indicating that very early during the densification process, the two clones have separated into distinct glass basins in which each of them is becoming trapped. This is due to the fact that the initial configuration at $\varphi_\ell = 0.565$ is not dynamically arrested, leaving each clone free to diffuse in a different direction in phase space.

The results for the crunch from the liquid phase are summarised in Fig. 2d, where we report the values of $\Delta_{AB}(t_w)$ and the long time limit of $\Delta(t,t_w)$, for several values of t_w, as a function of pressure P. We observe that at all pressures, $\Delta_{AB}(t_w)$ remains much larger than $\Delta(t,t_w)$, and the separation increases with increasing t_w, corresponding to the fact that, while aging proceeds, individual clones are increasingly trapped into distinct regions of phase space.

3.2 Dynamics from the dynamically arrested liquid phase

In Fig. 2e, we report the evolution of the packing fraction $\varphi(t_w)$ after a crunch from the dynamically arrested liquid phase, at initial density $\varphi_{g_1} = 0.619$. In this case, the dynamics is very different. At all pressures P, the density quickly reaches a stationary value, i.e. $\varphi(t_w)$ is independent of t_w. This long-time value is reported in the phase diagram of Fig. 1 as a function of pressure. This line defines the *equation of state* of the glass basin selected by the initial (dynamically arrested) configuration, followed out of equilibrium as a function of the imposed pressure[50]. Our results are consistent with a previous determination, obtained in Ref. 56.

In Fig. 2f, we report the dynamics of the MSD $\Delta(t,t_w)$ after the crunch from φ_{g_1}, which is also very different than the one from the liquid. For pressures slightly larger, but close to the initial equilibrium value (e.g. $P = 46$), after a short initial transient, no aging is observed. The MSD becomes stationary, i.e. $\Delta(t,t_w)$ is independent of t_w, but it shows no diffusive behavior at large times t. Instead, the plateau extends at infinite times, indicating that the system has reached equilibrium within a restricted portion of phase space that defines a *glass basin*[26,29]. The same behavior is observed for all pressures $P \lesssim 97$. For pressures $P \approx 97$ and above, a different behavior is observed: the plateau does not extend to infinite times, but at large values of t the MSD departs from the plateau to reach higher values, in a t_w-dependent manner. However, a fully diffusive regime is never observed, and the MSD seems to saturate at a higher plateau. These results are consistent with the expectation based on mean field theory in presence of a Gardner transition[29], and with the numerical results of Refs. 55,56.

In Fig. 2g, we report the dynamics of the MSD between different clones, $\Delta_{AB}(t_w)$. We find that, differently from the crunch

This journal is © The Royal Society of Chemistry [year]

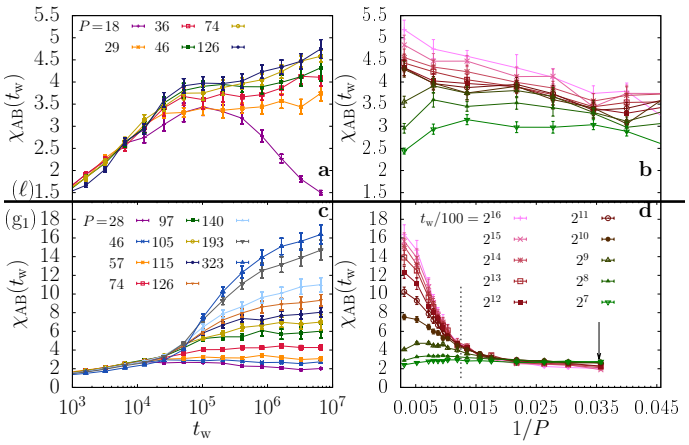

Fig. 3 Clone (spin-glass) susceptibility. We show the values of the susceptibility defined in Eq.(4) for the ergodic liquid ($\varphi_\ell = 0.565$) as function of t_w in (a) and for different t_w as function of $1/P$ in (b). In the bottom panels (c,d) we show the same curves for the dynamically arrested liquid ($\varphi_{g1} = 0.619$). While χ_{AB} is essentially insensitive to all t_w and P in the liquid, in the glass this behavior is only observed at low pressures, and a strong growth of the susceptibility is observed for $P \gtrsim 97$. As a guide to the eye, we have included the value of the position of the Gardner crossover for this φ_g estimated in Ref. 56 as a vertical dashed line, and an arrow to indicate the initial pressure.

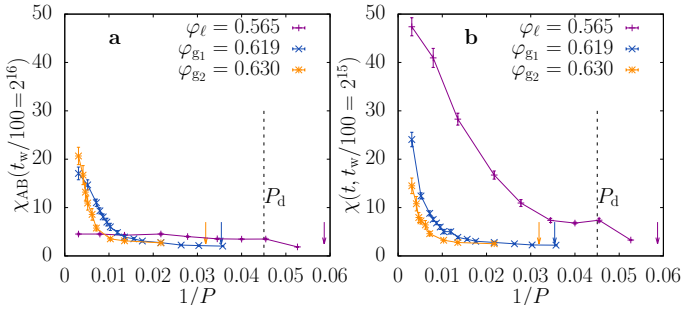

Fig. 4 Susceptibilities along the compression. We show $\chi_{AB}(t_w)$ (a) and $\chi(t,t_w)$ (b) for the largest accessible times, as functions of $1/P$, for the three compression lines studied. We include the position of the dynamical transition P_d as a vertical dashed line.

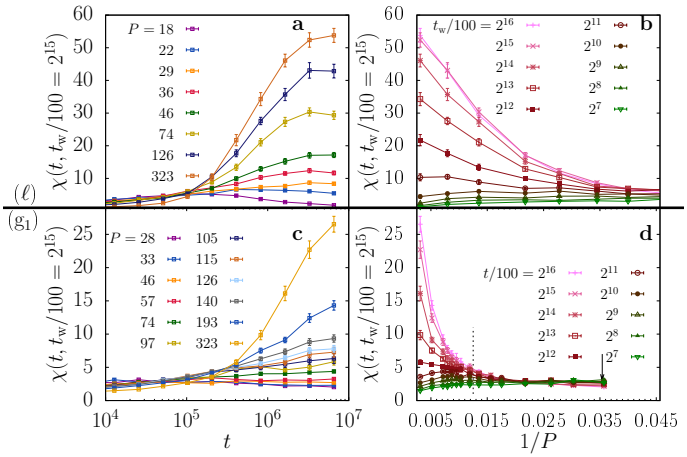

Fig. 5 Dynamical susceptibility. We show the values of the dynamical susceptibility defined in Eq.(4), for the largest available t_w, as function of t in (a,c) and for different t as function of $1/P$ in (b,d). Contrary to Fig. 3, a strong dependence of χ with P and t_w is observed in the crunch from the ergodic liquid (a,b), which corresponds to the well-known dynamical heterogeneities. The curves for the dynamically arrested liquid ($\varphi_{g1} = 0.619$) are shown in (c,d) displaying the same qualitative behavior than χ_{AB}.

from the liquid, in this case $\Delta_{AB}(t_w)$ overshoots, as an effect of the compression, and then saturates to a small value, that is always of the same order of magnitude as $\Delta(t,t_w)$. In particular, for the lower pressures $P \lesssim 97$, the long t_w limit of $\Delta_{AB}(t_w)$ coincides with the long t limit of $\Delta(t,t_w)$ (which is independent of t_w for large enough t_w), indicating that the glass basins is sampled ergodically[8,29,50,55,56]. Around $P \approx 97$, the long time limits of $\Delta_{AB}(t_w)$ and $\Delta(t,t_w)$ separate, while remaining of the same order of magnitude, indicating that the two clones are falling into distinct sub-regions of the same glass basin[55–59].

To highlight this separation process, in Fig. 2h we report the values of $\Delta_{AB}(t_w)$ and the long time limit of $\Delta(t,t_w)$, for several values of t_w, as a function of pressure P. The two values coincide at all t_ws for $P \lesssim 97$ (with the exception of the liquid point where some remanent diffusion is observed at the longest times), while they separate above this value, their separation increasing upon increasing t_w. This indicates that a sharp dynamical crossover is taking place around $P \approx 97$, which defines the (average) Gardner crossover point for the glass basins selected at initial density φ_{g_1}. The results for the other initial density φ_{g_2}, which can be found in the Appendix, are qualititatively similar, with the only difference that the Gardner crossover is shifted to higher pressures[56].

In summary, the analysis of the dynamical evolution of the density and of the MSD after a sudden crunch allows one to clearly distinguish between *(i)* the standard aging from the liquid phase at φ_ℓ, which is observed at all pressures and corresponds to each clone sampling independently the emergence of distinct metastable "threshold" states, and *(ii)* the aging from a dynamically arrested liquid configuration at φ_{g_1} or φ_{g_2}, which is only observed at pressures larger than a well-defined crossover point, and corresponds to the same glass basin breaking into a set of distinct sub-regions, explored by distinct clones.

3.3 Clone (spin-glass) susceptibility

The structure of sub-regions observed within the glass basin might be due to localised defects, i.e. small groups of particles that can be in two distinct local energy minima, leading to small barriers[57,58,74,75], or to extended defects, leading to collective rearrangements and higher barriers, as predicted by mean field in spin-glasses[16] and in particle systems[29,42]. A good way to discriminate between these two scenarios is to investigate the susceptibility $\chi_{AB}(t_w)$ defined in Eq. (4), associated to the displacement between distinct clones, also known as spin-glass susceptibility in spin-glass physics. A small value of $\chi_{AB}(t_w)$ indicates small spatial correlations, suggesting localised defects[57,58], while a large $\chi_{AB}(t_w)$ indicates large-scale spatially correlated, collective excitations[56].

In Fig. 3a we report $\chi_{AB}(t_w)$ as a function of t_w for several pressures, for a crunch from the ergodic liquid at initial density $\varphi_\ell = 0.565$. In Fig. 3b, the same data are plotted as a function

of $1/P$ for several values of t_w. For the lowest pressure $P = 19$, $\chi_{AB}(t_w)$ grows but then reaches a maximum and decreases, indicating full decorrelation of the clones at long times. This behavior is reminiscent of the well-studied dynamical heterogeneities that characterise the liquid phase upon approaching the dynamical transition[23,76]. For larger pressures, the susceptibility is always increasing with t_w, but the growth is modest (approximately a factor of 2) and roughly independent of pressure. In Fig. 3b it is clearly seen that the aging is qualitatively similar at all pressures, and no crossover is detected. This is consistent with Fig. 2b and with the standard properties of aging after a quench from the liquid phase, in which distinct clones are expected to explore distinct (hence uncorrelated) threshold states[72]. Note that the existence of a Gardner-like crossover in this regime has been proposed in Ref. 14, but the crossover is expected to be very weak and difficult to detect in numerical simulations. We leave a more detailed investigation of this crossover for future work.

A very different behavior is observed when the crunch is from the dynamically arrested phase, at $\varphi_{g_1} = 0.619$, as reported in Fig. 3c. In this case, at low pressure $\chi_{AB}(t_w)$ is roughly constant, while at high pressure we observe a sharp and continuous increase of $\chi_{AB}(t_w)$ upon increasing t_w, by a factor of ≈ 10 for the largest pressures, over the accessible time window. The growth is initially faster, and then crosses over to a slower regime, roughly logarithmic in t_w. The same data are shown in Fig. 3d as a function of $1/P$ for several t_w, which makes clear that there is a sharp crossover around $P \approx 97$, as observed in the MSD. For $P \lesssim 97$, no growth of $\chi_{AB}(t_w)$ is observed, while a sharp growth is observed for $P \gtrsim 97$. While we do not observe a sharp divergence of the susceptibility, the crossover point is roughly consistent with the values reported in Ref. 56, where the crossover was estimated by a different method.

To summarize these results, in Fig. 4a we report $\chi_{AB}(t_w)$ for the largest t_w, as a function of inverse pressure $1/P$, for the crunches from the three initial states at φ_ℓ, φ_{g_1}, and φ_{g_2}. This plot clearly shows that no correlation between clones is observed in the crunch from the ergodic liquid, while a large correlation builds up in the crunches from the dynamically arrested phase, below the Gardner crossover. Furthermore, the Gardner crossover is found to shift at higher pressures for denser initial states, consistently with the theory[27,29,50] and with earlier numerical results on the same system[56] illustrated in Fig. 1.

3.4 Dynamical susceptibility

The clone susceptibility $\chi_{AB}(t_w)$ is easily studied in numerical simulations, but it is very hard to measure in experiments, because one cannot prepare two clones of the system starting in the same initial configurations with different velocities. A solution that was adopted in the granular experiment of Seguin and Dauchot[59] was to perform compression/decompression cycles. Here, we discuss another possible solution, which consists in investigating the dynamical susceptibility $\chi(t, t_w)$ for a single clone of the system. This observables is straightforward to measure in experiments, provided one is able to repeat the experiment a sufficient number of times to obtain a proper averaging over clones or samples.

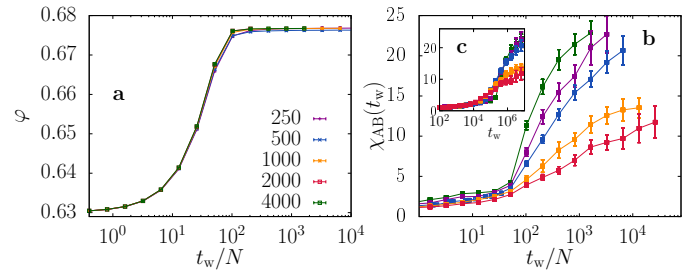

Fig. 6 Finite size effects. For the case $\varphi_{g_2} = 0.630$, we show in (a) the evolution of packing fraction φ for different system sizes N as a function of the scaled variable t_w/N. The curves collapse, showing that the compression rate is N dependent in our set-up. In figure (b) we show χ_{AB} for different N as function of the same variable, showing that the curves collapse during the compression (short times) but not at longer times, where the density stabilises to its final value. In this regime, larger N have slower compression rates, hence older effective age, corresponding to a higher χ_{AB}. This effect might be mixed with genuine finite size effects. In the inset (c) we show the same curves but plotted versus the non-scaled t_w, showing that the higher system sizes roughly collapse to the same curve.

In Fig. 5 we report the dynamical susceptibility, for a fixed value of t_w (the largest one we can access), as a function of time t. In the case of a crunch from the ergodic liquid (Fig. 5a), the system performs standard aging, and the dynamical susceptibility is different from the clone one: it displays a maximum as a function of t, and then decreases, at least for the lowest pressures. For the higher pressures, we believe that the time scale at which $\chi(t, t_w)$ decreases has fallen outside the accessible time window. Also, the susceptibility reaches larger values. This is associated to the well know dynamical heterogeneities that develop in this regime[23,76]. When plotted as a function of inverse pressure $1/P$ (Fig. 5b), the susceptibility is found to be time-dependent at all pressures, and no sharp crossover is visible, confirming that in this case the aging is qualitatively similar at all pressures.

Instead, in the case of a crunch from the dynamically arrested phase (Fig. 5b), the behavior of $\chi(t, t_w)$ is qualitatively very similar to the one of the clone susceptibility reported in Fig. 3. When plotted as a function of inverse pressure $1/P$ (Fig. 5d), the susceptibility is found to increase with t at pressures larger than the Gardner crossover, and to remain small and independent of t at pressure below it. We thus conclude that in this case a dynamical susceptibility measurement, for an appropriate value of t_w, provides similar information to a measurement of the clone susceptibility. A direct comparison of the two susceptibilities is given in Fig. 4.

3.5 Finite size effects

In Fig. 6 we discuss the robustness of our results against finite size effects by varying the number of particles N. As discussed in Section 2, the constant-pressure Monte Carlo code uses moves of $\delta V \propto 1/N$ in order to keep a constant acceptance rate. As a result, the compression rate scales as $1/\delta V \propto N$ as we show in Fig. 6a where the densification process is found to be independent of system size, once the time is rescaled by N. We show $\chi_{AB}(t_w)$ as function of the same scaling variable in Fig. 6b, showing that

This journal is © The Royal Society of Chemistry [year]

all curves collapse at short times, during the compression process. At longer times, once $\varphi(t_w)$ has stabilised, larger system display a faster growth of the susceptibility, which is unexpected. Indeed, as long as the correlation length $\xi(t_w)$ remains much lower than the linear size of the simulation box L, the growing of the amorphous domains should be independent of N. It might be that the linear size is not large enough to eliminate completely the finite size effects: indeed, in spin-glasses it has been estimated that one needs to simulate systems with $L > 7\xi(t_w)$ in order to avoid these effects[77]. This observation might also be related to our simulation set-up: larger systems have slower compression rate, hence larger effective age, corresponding to larger $\chi_{AB}(t_w)$. Indeed, while the compression is N-dependent, the exploration of the cages is not, which makes hard to compare the different system sizes at the same physical time. In fact, if we plot the same curves as a function of t_w instead of t_w/N (Fig. 6c), we can see that the curves for the two largest N collapse. Based on this discussion, we believe that the use of the value of $N = 1000$ is enough for the purpose of our investigation.

4 Results: spin glass

4.1 Details of the simulation

To obtain a direct comparison of hard spheres and a spin-glass in a field, we performed Monte Carlo simulations of an Edwards-Anderson spin-glass model in an external magnetic field[16], using the Metropolis algorithm. Our $3d$ system is defined on a cubic lattice with linear size $L = 24$ and periodic boundary conditions. The Hamiltonian is

$$\mathscr{H} = -\sum_{\langle i,j \rangle} J_{ij} s_i s_j - H \sum_i s_i \ , \tag{5}$$

where $s_i = \pm 1$ are spin variables located on the vertices of the lattice, the first sum is over nearest neighbors on the lattice, and the J_{ij} are i.i.d. quenched random variables that take the value ± 1 with equal probability. We studied the system with fields $H = 0.1$ and $H = 0.2$. For each value of temperature and field, we simulate $N_s = 1280$ samples (independent realisation of the disorder J_{ij}) and $N_c = 4$ clones. Each clone is prepared at $t_w = 0$ at infinite temperature, i.e. in a random spin configuration, and instantaneously quenched at the final temperature T, where its dynamical evolution is followed.

4.2 Mapping between spin-glasses and structural glasses

In Fig. 7 we report the overlap dynamics of the spin-glass, where the overlap $q(t,t_w) = (1/N)\sum_i \langle s_i(t+t_w) s_i(t_w) \rangle$ is equal to 1 for identical configurations $\{s_i(t_w)\}$ and $\{s_i(t_w+t)\}$, and smaller than 1 otherwise. The quantity $1 - q(t,t_w)$ is then equivalent of the mean-square displacement for particle systems, as both quantities measure the distance in phase space between configurations, and both increase for increasingly different configurations. The same reasoning can be applied to the clone overlap $q_{AB}(t_w) = (1/N)\sum_i \langle s_i^A(t_w) s_i^B(t_w) \rangle$.

For both values of the external field H, we observe that at high temperature the clone overlap converges to a value independent of t_w, while the dynamical overlap becomes t_w independent and its long time limit $q(t \to \infty, t_w \to \infty)$ coincides with the one of $q_{AB}(t_w \to \infty)$ (Fig. 7a,d). This implies that phase space is sampled ergodically in the high temperature phase. Upon lowering the temperature, for both values of H, we observe that a second plateau emerges in $q(t,t_w)$, and aging appears at large values of t (Fig. 7a,d). Correspondingly, the long-time limits of $q(t,t_w)$ and $q_{AB}(t_w)$ separate (Fig. 7b,e). The separation becomes more evident when the long time limits are plotted as a function of temperature (Fig. 7c,f). The dynamical crossover temperature is lower for larger values of magnetic field.

Based on these results, let us discuss briefly the mapping between structural glasses and spin-glasses in an external field, referring to Refs. 61,62 for more details. In spin-glasses, a realisation of the quenched disorder J_{ij} defines a sample. Each sample has a single ergodic (paramagnetic) free energy basin at high temperature, and undergoes a crossover to a non-ergodic fractured (spin-glass) basin at low temperatures. In structural glasses, the role of quenched disorder is played by the initial condition, provided one is in the dynamically arrested phase. In that phase, each initial configuration belongs to a single glass basin, that can be identified with the paramagnetic basin of the spin-glass. Upon increasing pressure, the glass basin fractures into a non-ergodic basin, akin to the spin-glass phase. The similarity of the spin-glass results in Fig. 7 with the structural glass ones in Fig. 2 (lower line, corresponding to a crunch from the dynamically arrested liquid) confirm this picture.

Note that this reasoning does not hold for the structural glass if the initial configuration is in the ergodic liquid phase. In that case, the initial configuration does not belong to a glass free energy basin: it is free to explore all the liquid phase space, and upon compression the physics is very different, as metastable states form abruptly and trap the dynamics giving rise to a standard discontinuous glass transition. The observed phenomenology (Fig. 2, upper line) is, indeed, different.

4.3 Spin-glass susceptibility

In Fig. 8a,c we report the spin-glass susceptibility

$$\chi_{SG}(t_w) = \overline{\left[\sum_{ij} [\langle u_i(t_w) u_j(t_w) \rangle - \langle u_i(t_w) \rangle \langle u_j(t_w) \rangle] \right]} \ , \tag{6}$$

with $u_i(t_w) = s_i^A(t_w) s_i^B(t_w)$, which is the equivalent of the clone susceptibility for the hard sphere case. For both values of the field H, we observe that at high temperature the susceptibility is roughly constant. Upon lowering the temperature, the susceptibility starts increasing with t_w, and it saturates to a larger and larger value. At some point, the saturation time exceeds the accessible time of the simulation, and the susceptibility constantly increases in a roughly logarithmic manner. For even lower temperature, we observe that the increase remains roughly logarithmic, but with a smaller and smaller prefactor, indicating that the aging slows down. The latter phenomenon is not observed in our hard sphere samples. We presume that this is due to the fact that we cannot reach sufficiently large pressures.

The same data can be plotted as a function of T for various t_w

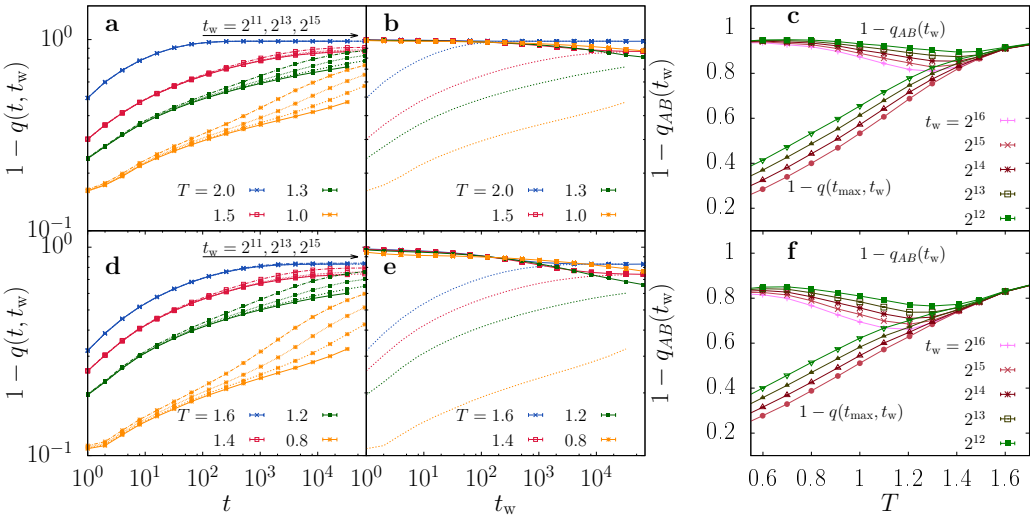

Fig. 7 Overlap dynamics after a sudden quench for the spin glass in a field. We show the dynamics of $1-q(t,t_w)$ and $1-q_{AB}(t_w)$ for two different values of the external field, $H=0.1$ (top panels) and $H=0.2$ (bottom panels). In figures (a,d) we plot $1-q(t,t_w)$ as function of t for different values of t_w after the instantaneous quench in temperature. In figure (a) aging is visible for $T \lesssim 1.6$ while in (d) it appears at $T \lesssim 1.4$. In (b,e) we show $1-q(t,t_w)$ as function of t for the highest available t_w, together with $1-q_{AB}(t_w)$ as function of t_w. One can observe that both curves converge to the same asymptote for temperatures above the onset of aging and differ by much below it. In panels (c,f) we show the value of $1-q(t,t_w)$ corresponding to the largest time in (b,e), together with $1-q_{AB}(t_w)$ as a function of T for several t_w, which shows the separation at the onset of aging.

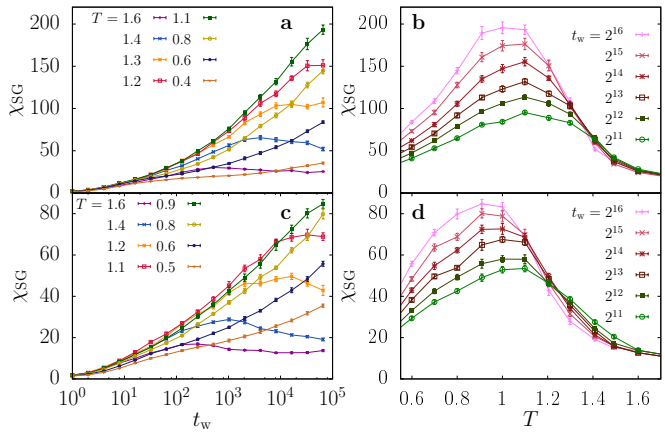

Fig. 8 Susceptibility for the spin glass in a field. We show results for the spin glass susceptibility in a field defined in Eq. (6) for two different values of the field $H=0.1$ (top panels) and $H=0.2$ (bottom panels). In panels (a,c) we show the evolution with t_w for different temperatures and in (b,d) the same data but plotted versus T for several t_w.

(Fig. 8b,d). For small t_w, the susceptibility displays a maximum around the point where aging begins (the equivalent of the Gardner crossover), once again due to the fact that the aging slows down at very low temperatures. Upon increasing t_w, the maximum grows and shifts progressively to lower temperatures. Note that this maximum is only observed in the hard sphere case at short t_w (see e.g. the data for $t_w/100 = 2^9$ in Fig. 3d), presumably, as already mentioned, because of the limited range of pressures: upon increasing t_w the maximum shifts to higher pressures and falls out of the accessible range.

5 Conclusions

In this paper, we studied the dynamics of a polydisperse $3d$ hard sphere glass. The glass was prepared either in the ergodic liquid phase, at densities below the dynamical (or MCT) transition, or in the dynamically arrested phase above it. Then, the system was instantaneously crunched to a higher pressure, and the subsequent aging dynamics was investigated.

The crunch dynamics from the ergodic liquid phase is in agreement with previous studies performed in this regime. Different realisations of the dynamics (clones) evolve towards decorrelated *threshold* states, that progressively trap the dynamics. The distance between clones $\Delta_{AB}(t_w)$ is large, while the mean square displacement $\Delta(t,t_w)$ of a single clone displays aging at all pressures. The clone susceptibility $\chi_{AB}(t_w)$ is featureless, while the dynamical susceptibility $\chi(t,t_w)$ grows at all pressures indicating the presence of dynamical heterogeneities, which, in mean field, is due to the criticality of the threshold states[72].

The crunch dynamics from the dynamically arrested phase is instead very different. Here, initial configurations are already trapped in a glass basin before the crunch. If the crunch is to a pressure moderately higher than the initial one, $P \lesssim P_G$, then one observes a fast relaxation dynamics to a new state in which the glass basin is ergodically sampled at the higher pressure. In this case, no aging is observed and the susceptibilities remain small. Furthermore, the long time limits of $\Delta_{AB}(t_w \to \infty)$ and $\Delta(t \to \infty, t_w \to \infty)$ coincide, and the same happens for the susceptibilities. By crunching at higher pressures $P \gtrsim P_G$, we observe instead that the glass basin becomes fractured in sub-basins, leading to the emergence of long time scales, and the associated aging. At the same time, the susceptibilities grow, indicating the cooperative nature of the excitations that lead to crossing barriers between sub-states in a basin.

This journal is © The Royal Society of Chemistry [year]

We identify the pressure P_G as a Gardner crossover, reminiscent of the Gardner phase transition predicted by mean field theory[27,29]. However, we note that in our $3d$ simulations the growth of the susceptibility $\chi_{AB}(t_w)$ with t_w is very slow (logarithmic in time), which hinders the possibility of observing large values of $\chi_{AB}(t_w)$ and thus deciding whether P_G is a real phase transition or just a sharp dynamical crossover.

The situation is very similar to the case of spin-glasses in an external magnetic field, where mean field predicts a sharp second-order phase transition[16], while numerical simulations observe a slowly growing spin-glass susceptibility and are unable to decide on the existence of a transition[78]. When plotting $\chi_{SG}(t_w)$ as a function of T, one observes a maximum that slowly grows with increasing t_w (suggesting a phase transition), but also slowly shifts to lower temperatures (suggesting that the critical point might be only at $T = 0$). Unfortunately, both processes happen very slowly (logarithmically) with increasing t_w, so that it is not possible to extract reliably the asymptotic behavior. While on the observational time scales, it is clear that some cooperative phenomenon is taking place, deciding on whether this phenomenon is of thermodynamical or dynamical nature is very difficult. Our data strongly suggest that the situation is very similar in the $3d$ hard sphere glasses, confirming that the two systems are in the same universality class, as suggested by theoretical arguments[48,61–63]. Unfortunately, due to the limited pressure range of the hard sphere simulation, the maximum in $\chi_{AB}(t_w)$ is less evident than in the spin-glass case.

Finally, we note that in the crunches from the dynamically arrested liquid phase, we find strong indications that the system is not able to leave the original glass basin in which it is trapped in equilibrium: the particle displacements always remain very small (less than a tenth of the average particle diameter, see Fig. 2f). Thus, no activated events in which the system jumps among distinct glass basins are observed in our simulations, which prevents us from testing the ideas developed in Ref. 66 about RFOT-like nucleation and the associated buckling instabilities in hard sphere glasses.

We conclude that $3d$ colloidal and granular glasses display spin-glass like aging beyond the Gardner crossover, located deeply in the off-equilibrium glass phase. The aging is associated to collective excitations that are responsible for many anomalies of the solid phase. Unfortunately, as in the spin-glass, equilibration times grow very fast, and a systematic study of the crossover as a function of system size and t_w is impossible with current computers. Yet, an interesting direction for future work would be to perform more systematic studies of the sample-to-sample fluctuations, that are known to be highly non-trivial in spin-glasses. Another interesting future direction would be to study the nature of the Gardner transition in equilibrium[62] as in the Edwards-Anderson model[78,79], using the replica exchange algorithm (parallel tempering) for small systems[80,81] (with temperature replaced by pressure). This might shed additional light on the nature of the crossover.

Acknowledgements

We wish to thank Ludovic Berthier, Patrick Charbonneau, Olivier Dauchot, Yuliang Jin, Mike Moore, Misaki Ozawa, Giorgio Parisi, Camille Scalliet, Pierfrancesco Urbani, Peter Wolynes, and Sho Yaida for many useful discussions. We thank Yuliang Jin for providing us the initial equilibrated configurations from Ref. 51. We thank the *Janus collaboration*, and in particular Marco Baity-Jesi, Luis Antonio Fernández and Víctor Martín-Mayor, for letting us use the PC version of the spin-glass simulation program used in Ref. 78.

This work was granted access to the high performance computer (HPC) resources of MesoPSL financed by the Region Ile de France and the project Equip@Meso (reference ANR-10-EQPX-29-01) of the programme Investissements d'Avenir supervised by the Agence Nationale pour la Recherche. This work benefited from access to the University of Oregon HPC, Talapas, and from *Memento* cluster, part of the Instituto Universitario de biocomputación y física de sistemas complejos at the Universidad de Zaragoza (Spain).

This project has received funding from the European Research Council (ERC) under the European Union's Horizon 2020 research and innovation programme (grant agreement n. 723955 - GlassUniversality). B.S. was partially supported through Grant No. FIS2015-65078-C2-1-P, jointly funded by MINECO (Spain) and FEDER (European Union).

Appendix

A Two quenches from the liquid phase

In the main text we showed three off-equilibrium glass equations of state corresponding to instantaneous compressions from two dynamically arrested liquid configurations and one ergodic liquid configuration. In general, one expects that all the quenches from the ergodic liquid phase are equivalent, but this is only true if the starting point is far enough from the dynamical transition point, here $\varphi_d \sim 0.594$. To study this effect, we have also repeated the same protocol described in the main text, but this time starting from equilibrium ergodic liquid configurations at $\varphi_{\ell_2} = 0.59$, which is relatively near φ_d. We show in Fig. A1 its off-equilibrium equation of state, together with the other three lines. From the data, it is clear that the new line extrapolates to a significantly higher jamming point, but also its slope becomes more similar to the one described by the two glass lines obtained from dynamically arrested configurations. Despite this, the dynamics along this ℓ_2-line are more similar to that of the crunches from the ergogic liquid discussed in the main text, as we show in Fig. A2. For completeness, we also include in Fig. A2 the data for the g_2-line not shown in the main text.

Notes and references

1 E. Gardner, *Nucl. Phys. B*, 1985, **257**, 747–765.
2 D. Gross, I. Kanter and H. Sompolinsky, *Phys. Rev. Lett.*, 1985, **55**, 304.
3 B. Derrida, *Physical Review Letters*, 1980, **45**, 79.
4 D. J. Gross and M. Mézard, *Nucl. Phys. B*, 1984, **240**, 431.

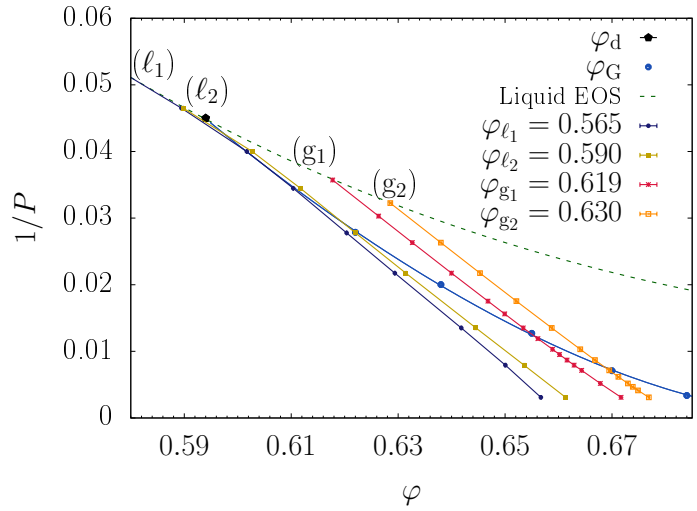

Fig. A1 Two quenches from the liquid. Same as Fig. 1 but this time adding a second quench from the ergodic liquid phase, starting at $\varphi_{\ell_2} = 0.59$

5 T. R. Kirkpatrick and P. G. Wolynes, *Phys. Rev. B*, 1987, **36**, 8552–8564.
6 T. R. Kirkpatrick and D. Thirumalai, *Phys. Rev. A*, 1988, **37**, 4439–4448.
7 T. Castellani and A. Cavagna, *J. Stat. Mech.*, 2005, **2005**, P05012.
8 S. Franz and G. Parisi, *J. Phys. I*, 1995, **5**, 1401–1415.
9 A. Barrat, R. Burioni and M. Mézard, *J. Phys. A*, 1996, **29**, L81.
10 A. Barrat, S. Franz and G. Parisi, *J. Phys. A*, 1997, **30**, 5593–5612.
11 F. Krzakala and L. Zdeborová, *EPL*, 2010, **90**, 66002.
12 L. Zdeborová and F. Krzakala, *Phys. Rev. B*, 2010, **81**, 224205.
13 A. Montanari and F. Ricci-Tersenghi, *Phys. Rev. B*, 2004, **70**, 134406.
14 T. Rizzo, *Phys. Rev. E*, 2013, **88**, 032135.
15 G. Parisi, *Physical Review Letters*, 1979, **43**, 1754.
16 M. Mézard, G. Parisi and M. A. Virasoro, *Spin glass theory and beyond*, World Scientific, Singapore, 1987.
17 T. R. Kirkpatrick and P. G. Wolynes, *Phys. Rev. A*, 1987, **35**, 3072–3080.
18 T. R. Kirkpatrick and D. Thirumalai, *Phys. Rev. Lett.*, 1987, **58**, 2091–2094.
19 T. R. Kirkpatrick and D. Thirumalai, *Phys. Rev. B*, 1987, **36**, 5388–5397.
20 T. R. Kirkpatrick, D. Thirumalai and P. G. Wolynes, *Phys. Rev. A*, 1989, **40**, 1045–1054.
21 M. Mezard and G. Parisi, Structural Glasses and Supercooled Liquids: Theory, Experiment and Applications, 2012.
22 A. Cavagna, *Physics Reports*, 2009, **476**, 51–124.
23 L. Berthier and G. Biroli, *Rev. Mod. Phys.*, 2011, **83**, 587–645.
24 *Structural Glasses and Supercooled Liquids: Theory, Experiment, and Applications*, ed. P. Wolynes and V. Lubchenko, Wiley, 2012.
25 G. Parisi and F. Zamponi, *J. Stat. Mech.*, 2006, **2006**, P03017.
26 G. Parisi and F. Zamponi, *Rev. Mod. Phys.*, 2010, **82**, 789–845.
27 J. Kurchan, G. Parisi, P. Urbani and F. Zamponi, *J. Phys. Chem. B*, 2013, **117**, 12979–12994.
28 T. Maimbourg, J. Kurchan and F. Zamponi, *Phys. Rev. Lett.*, 2016, **116**, 015902.
29 P. Charbonneau, J. Kurchan, G. Parisi, P. Urbani and F. Zamponi, *Annual Review of Condensed Matter Physics*, 2017, **8**, 265–288.
30 A. J. Liu and S. R. Nagel, *Nature*, 1998, **396**, 21–22.
31 C. S. O'Hern, S. A. Langer, A. J. Liu and S. R. Nagel, *Phys. Rev. Lett.*, 2002, **88**, 075507.
32 C. S. O'Hern, L. E. Silbert, A. J. Liu and S. R. Nagel, *Phys. Rev. E*, 2003, **68**, 011306.
33 L. Silbert, A. Liu and S. Nagel, *Phys. Rev. Lett.*, 2005, **95**, 098301.
34 M. Wyart, L. Silbert, S. Nagel and T. Witten, *Phys. Rev. E*, 2005, **72**, 051306.
35 M. Wyart, *Annales de Physique*, 2005, **30**, 1–96.
36 C. Brito and M. Wyart, *Europhysics Letters (EPL)*, 2006, **76**, 149–155.
37 C. Brito and M. Wyart, *J. Stat. Mech.*, 2007, **2007**, L08003.
38 A. Liu, S. Nagel, W. Van Saarloos and M. Wyart, Dynamical Heterogeneities and Glasses, Oxford, 2011.
39 A. J. Liu and S. R. Nagel, *Annu. Rev. Condens. Matter Phys.*, 2010, **1**, 347–369.
40 M. Wyart, *Phys. Rev. Lett.*, 2012, **109**, 125502.
41 M. Müller and M. Wyart, *Ann. Rev. Cond. Matt. Phys.*, 2015, **6**, 177–200.
42 P. Charbonneau, J. Kurchan, G. Parisi, P. Urbani and F. Zamponi, *Nat. Comm.*, 2014, **5**, 3725.
43 P. Charbonneau, E. I. Corwin, G. Parisi and F. Zamponi, *Phys. Rev. Lett.*, 2015, **114**, 125504.
44 C. P. Goodrich, A. J. Liu and S. R. Nagel, *Phys. Rev. Lett.*, 2012, **109**, 095704.
45 E. DeGiuli, A. Laversanne-Finot, G. Düring, E. Lerner and M. Wyart, *Soft Matter*, 2014, **10**, 5628–5644.
46 S. Franz, G. Parisi, P. Urbani and F. Zamponi, *Proc. Nat. Acad. Sci. U.S.A.*, 2015, **112**, 14539–14544.
47 H. Mizuno, H. Shiba and A. Ikeda, *Proceedings of the National Academy of Sciences*, 2017, **114**, E9767.
48 G. Biroli and P. Urbani, *Nature Physics*, 2016, **12**, 1130.
49 H. Yoshino and F. Zamponi, *Phys. Rev. E*, 2014, **90**, 022302.
50 C. Rainone, P. Urbani, H. Yoshino and F. Zamponi, *Phys. Rev. Lett.*, 2015, **114**, 015701.
51 Y. Jin and H. Yoshino, *Nature communications*, 2017, **8**, 14935.
52 P. Urbani and F. Zamponi, *Physical review letters*, 2017, **118**, 038001.
53 S. Franz and S. Spigler, *Physical Review E*, 2017, **95**, 022139.
54 N. Xu, V. Vitelli, A. J. Liu and S. R. Nagel, *Europhys. Lett.*, 2010, **90**, 56001.

This journal is © The Royal Society of Chemistry [year]

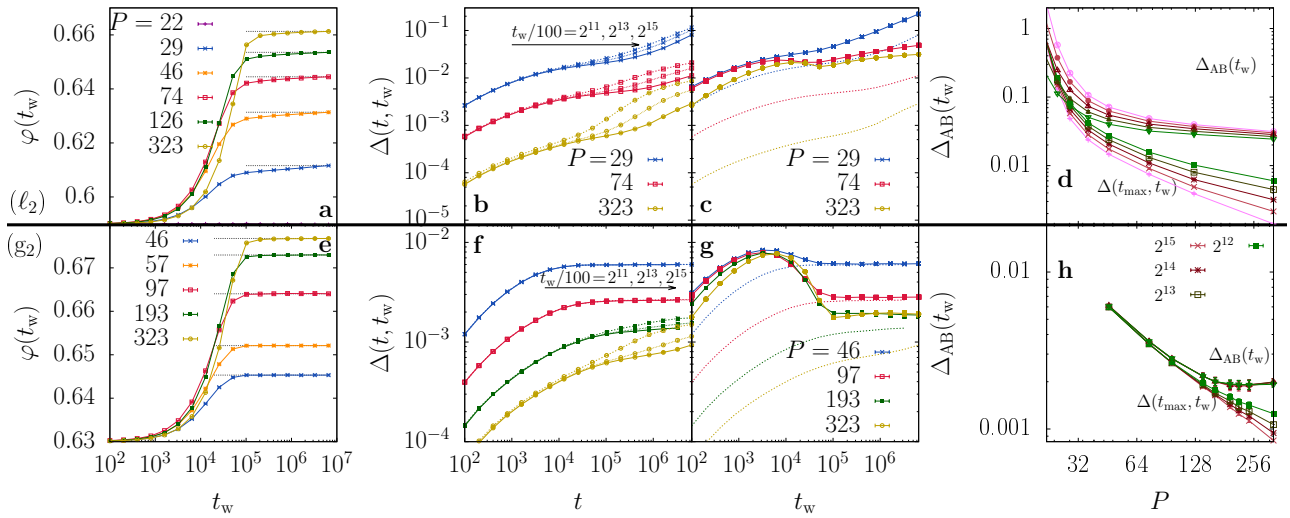

Fig. A2 Dynamics after a crunch for the additional lines. Same as Fig. 2 for the two other initial states, $\varphi_{\ell_2} = 0.59$ (top) and $\varphi_{g_2} = 0.630$ (bottom).

55 P. Charbonneau, Y. Jin, G. Parisi, C. Rainone, B. Seoane and F. Zamponi, *Phys. Rev. E*, 2015, **92**, 012316.

56 L. Berthier, P. Charbonneau, Y. Jin, G. Parisi, B. Seoane and F. Zamponi, *Proceedings of the National Academy of Sciences*, 2016, **113**, 8397–8401.

57 C. Scalliet, L. Berthier and F. Zamponi, *Physical review letters*, 2017, **119**, 205501.

58 B. Seoane, D. R. Reid, J. J. de Pablo and F. Zamponi, *Physical Review Materials*, 2018, **2**, 015602.

59 A. Seguin and O. Dauchot, *Physical review letters*, 2016, **117**, 228001.

60 K. Geirhos, P. Lunkenheimer and A. Loidl, *Physical Review Letters*, 2018, **120**, 085705.

61 C. J. Fullerton and M. Moore, *arXiv:1304.4420*, 2013.

62 P. Urbani and G. Biroli, *Phys. Rev. B*, 2015, **91**, 100202.

63 P. Charbonneau and S. Yaida, *Physical Review Letters*, 2017, **118**, year.

64 C. L. Hicks, M. J. Wheatley, M. J. Godfrey and M. A. Moore, *arXiv:1708.05644*, 2017.

65 M. Baity-Jesi, R. A. Baños, A. Cruz, L. A. Fernandez, J. M. Gil-Narvion, A. Gordillo-Guerrero, D. Iñiguez, A. Maiorano, F. Mantovani, E. Marinari, V. Martin-Mayor, J. Monforte-Garcia, A. Muñoz Sudupe, D. Navarro, G. Parisi, S. Perez-Gaviro, M. Pivanti, F. Ricci-Tersenghi, J. J. Ruiz-Lorenzo, S. F. Schifano, B. Seoane, A. Tarancon, R. Tripiccione and D. Yllanes, *Physical Review E - Statistical, Nonlinear, and Soft Matter Physics*, 2014, **89**, 032140.

66 V. Lubchenko and P. G. Wolynes, *The Journal of Physical Chemistry B*, 2018, **122**, 3280–3295.

67 L. Berthier, D. Coslovich, A. Ninarello and M. Ozawa, *Physical review letters*, 2016, **116**, 238002.

68 S. Mossa, G. Ruocco, F. Sciortino and P. Tartaglia, *Philosophical Magazine B*, 2002, **82**, 695–705.

69 R. Di Leonardo, L. Angelani, G. Parisi and G. Ruocco, *Physical Review Letters*, 2000, **84**, 6054.

70 D. J. Amit and V. Martin-Mayor, *Field theory, the renormalization group, and critical phenomena: graphs to computers*, World Scientific Publishing Co Inc, 2005.

71 M. Baity-Jesi, E. Calore, A. Cruz, L. A. Fernandez, J. M. Gil-Narvion, A. Gordillo-Guerrero, D. Iñiguez, A. Maiorano, E. Marinari, V. Martin-Mayor, J. Moreno-Gordo, A. Muñoz-Sudupe, D. Navarro, G. Parisi, S. Perez-Gaviro, F. Ricci-Tersenghi, J. J. Ruiz-Lorenzo, S. F. Schifano, B. Seoane, A. Tarancon, R. Tripiccione and D. Yllanes, *arXiv:1803.02264*, 2018.

72 L. F. Cugliandolo and J. Kurchan, *Phys. Rev. Lett.*, 1993, **71**, 173–176.

73 M. Ozawa, T. Kuroiwa, A. Ikeda and K. Miyazaki, *Physical Review Letters*, 2012, **109**, 205701.

74 M. Goldstein, *J. Chem. Phys.*, 1969, **51**, 3728–3739.

75 A. Heuer, *J. Phys.: Condens. Matter*, 2008, **20**, 373101.

76 L. Berthier, G. Biroli, J. P. Bouchaud, L. Cipelletti and W. van Saarloos, *Dynamical Heterogeneities and Glasses*, Oxford University Press, Oxford, 2011.

77 F. Belletti, M. Cotallo, A. Cruz, L. A. Fernandez, A. Gordillo-Guerrero, M. Guidetti, A. Maiorano, F. Mantovani, E. Marinari, V. Martin-Mayor, A. Muñoz Sudupe, D. Navarro, G. Parisi, S. Perez-Gaviro, J. J. Ruiz-Lorenzo, S. F. Schifano, D. Sciretti, A. Tarancon, R. Tripiccione, J. L. Velasco and D. Yllanes, *Phys. Rev. Lett.*, 2008, **101**, 157201.

78 M. Baity-Jesi, R. A. Baños, A. Cruz, L. A. Fernandez, J. M. Gil-Narvion, A. Gordillo-Guerrero, D. Iñiguez, A. Maiorano, F. Mantovani, E. Marinari, V. Martin-Mayor, J. Monforte-Garcia, A. Muñoz Sudupe, D. Navarro, G. Parisi, S. Perez-Gaviro, M. Pivanti, F. Ricci-Tersenghi, J. J. Ruiz-Lorenzo, S. F. Schifano, B. Seoane, A. Tarancon, R. Tripiccione and D. Yllanes, *Journal of Statistical Mechanics: Theory and Experiment*, 2014, **2014**, P05014.

79 T. Jörg, H. Katzgraber and F. Krzakala, *Phys. Rev. Lett.*, 2008, **100**, 197202.

80 R. H. Swendsen and J.-S. Wang, *Physical Review Letters*, 1986,

57, 2607–2609.
81 E. Marinari and G. Parisi, *Simulated tempering: A New Monte Carlo Scheme*, 1992.

This journal is © The Royal Society of Chemistry [year]